Acta Crystallographica Section B
Structural Science
ISSN 0108-7681

Synchrotron X-ray analysis of the electron density in CoF_2 and ZnF_2

Nicholas J. O'Toole† and Victor A. Streltsov*

Crystallography Centre, The University of Western Australia, Nedlands 6907, Austalia

† Present address: Department of Cell and Molecular Pharmacology, Medical University of South Carolina, PO Box 250505, Charleston, SC 29425, USA.

Correspondence e-mail: strel@crystal.uwa.edu.au

Received 26 June 2000
Accepted 13 October 2000

Accurate structure factors for small crystals of the rutile-type structures CoF_2, cobalt difluoride, and ZnF_2, zinc difluoride, have been measured with focused $\lambda = 0.8400\ (2)$ Å synchrotron X-radiation at room temperature. Phenomenological structural trends across the full series of rutile-type transition metal difluorides are analysed, showing the importance of the metal atom in the degree of distortion of the metal–F_6 octahedra in these structures. Multipole models reveal strong asphericities in the electron density surrounding the transition metals, which are consistent with expectations from crystal field theory and the structural trends in these compounds. Transition metal 3*d*-orbital populations were computed from the multipole refinement parameters, showing significant repopulation of orbitals compared with the free atom, particularly for CoF_2.

1. Introduction

Several fluorides and oxides of fourth-period metals crystallize in the tetragonal rutile-type structure (space group $P4_2/mnm$) and display interesting optical and magnetic properties. Therefore, the structure has been studied extensively as a testing ground for quantum chemical theories of the electronic interactions in these materials.

In the rutile-type structure the metal atom is coordinated by a distorted octahedron of O or F ions (Fig. 1). The electronic basis of the structural distortions is traditionally described by Crystal Field Theory (*e.g.* Dunitz & Orgel, 1960), wherein the *d*-orbital degeneracy of the transition metal atom is lifted by the non-spherical potential due to the surrounding ligands. Some rutile-type structures can be qualitatively understood in terms of Jahn–Teller distortions (Burdett & Eisenstein, 1992). There are some modern theories relevant to the structure, which include consideration of metal–metal bonding effects. The reader is referred to the review by Burdett (1995) for further details.

The purpose of the present study is to accurately determine using synchrotron X-radiation the ground state electron density in two rutile-type structures, CoF_2 and ZnF_2, in order to relate observed electron density features to transition-metal orbital splitting and structural distortions. A series of recent experiments by our laboratory and collaborators (*e.g.* Streltsov *et al.*, 1998; Streltsov & Ishizawa, 1999) show the benefit of using synchrotron radiation for electron density imaging. Synchrotron radiation combines high flux with high-quality diffraction radiation and the use of small crystal samples reduces dramatically absorption and extinction.

There is a remarkable structural difference between antiferromagnetic CoF_2 and diamagnetic ZnF_2, which is revealed by inspection of these crystals' cell dimensions (Table 1).

There is a difference in the length of the *a* and *c* axes for the two structures – namely so that for CoF_2 the *a* axis is shorter and the *c* axis is longer than for ZnF_2 – in spite of the presumably similar size of Co and Zn atoms. The *c*/*a* ratio is 0.6771 (1) and 0.6662 (2) for CoF_2 and ZnF_2, respectively. It is desirable to understand the electronic basis for such structural effects by imaging the one-electron density. In CoF_2 significant asphericity in the electron density of the Co atom is expected due to preferential occupation of orbitals in the partially filled *d* subshell. On the other hand, features around the Zn atom in ZnF_2, which has a filled *d* subshell, should yield information on the subtle electronic processes causing structural distortions in this and other $3d^{10}$ compounds.

The electron densities in several rutile-type compounds have been determined experimentally, beginning with early studies of MgF_2 (Niederauer & Gottlicher, 1970) and rutile (TiO_2) itself (Shintani *et al.*, 1975). Of note amongst recent studies is an electron density analysis of NiF_2 and FeF_2 using γ-radiation by Palmer & Jauch (1993). Multipole model refinement for their data revealed significant asphericities in transition metal atoms. Data for NiF_2 was measured at room temperature and at 15 K, below its antiferromagnetic transition. The authors found virtually no effects on the electron density related to magnetic ordering. There is an impressive qualitative agreement between the Palmer & Jauch electron density maps for FeF_2 and those of Valerio *et al.* (1995). The latter maps were calculated theoretically using the *CRYSTAL*92 periodic Hartree–Fock code (Dovesi *et al.*, 1992).

Costa, de Almeida and co-workers (Costa & de Almeida, 1987; de Almeida *et al.*, 1989; Costa *et al.*, 1993) have performed a series of X-ray diffraction experiments on the transition metal fluorides VF_2, FeF_2, NiF_2 and CoF_2. All measurements were carried out at room temperature on a CAD-4 four-circle diffractometer. Small deviations from spherical symmetry for the 3*d*-metal atom are found in each material and fractional *d*-orbital populations were derived from the resultant electron density distributions. ZnF_2 crystals have never been the subject of an experimental electron density study before.

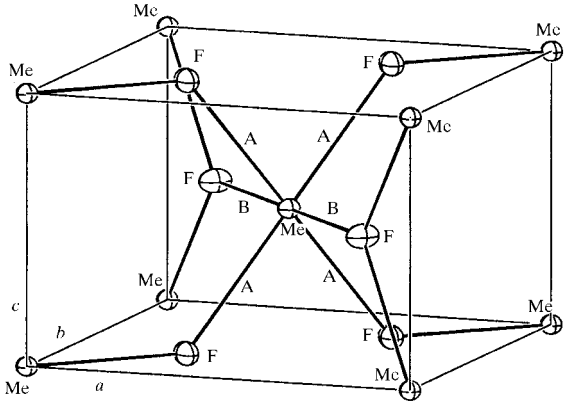

Figure 1
The rutile structure.

2. Experimental

2.1. Sample preparation

Single crystals of CoF_2 and ZnF_2 were grown from the melt by heating reagent-grade powders of the respective materials in sealed platinum crucibles at 1073 K. After fast cooling of the melt several small well formed crystals were found. The typical crystal shapes for both materials were rectangular prisms of approximate dimensions $50 \times 20 \times 20$ μm.

Crystals were pre-examined with a Siemens P4 four-circle diffractometer using a conventional Mo $K\alpha$ (λ = 0.71073 Å) tube X-ray source. The approximate orientation of each crystal was determined and recorded for subsequent use with the synchrotron radiation source. Crystals selected for the synchrotron radiation experiment were small (no dimension greater than approximately 50 μm) to reduce absorption and extinction effects. The limited size of such crystals meant that only the brightest reflections for each compound could be measured using the tube source for determination of crystal orientation.

The dimensions of each crystal were measured with an Electroscan ESEM-3 microscope. Indices and dimensions of bounding faces for each crystal are included in Table 1.[1]

2.2. Synchrotron data collection

Synchrotron X-ray diffraction data for the CoF_2 and ZnF_2 crystals were collected using the Beamline 14A (BL14A) four-circle diffractometer at the Photon Factory (Tsukuba, Japan). Experimental details are listed in Table 1. Vertically polarized radiation from a superconducting vertical wiggler was monochromated by a double Si (111) crystal monochromator and focused by a curved mirror. A high-speed avalanche photodiode (APD) detector with counting linearity up to 10^8 counts s^{-1} and estimated dead time less than 4 ns was used for the data collection at a wavelength of 0.8400 (2) Å. The detector, mounted on the 2θ arm of the BL-14A four-circle diffractometer, contained four epitaxic silicon avalanche photodiodes stacked perpendicular to the diffracted X-radiation. Each photodiode has a detection area of 2.8 mm in diameter with a thickness of ∼120 μm. The total intrinsic efficiency of the APD detector is 67.5% at 14.7 keV (0.84 Å). The reader is referred to Satow & Iitake (1989), Streltsov *et al.* (1998) or Kishimoto *et al.* (1998) for further technical details of BL14A's operation. Cell dimensions for each crystal were calculated from six reflections ($\pm$800, 0$\pm$80 and 00$\pm$6) with 2θ values of 91.38 and 104.86° for CoF_2, and 91.15 and 107.06° for ZnF_2. Reflection intensities were measured with ω–2θ continuous time scans over the complete sphere of reciprocal space up to $(\sin\theta/\lambda)_{max}$ values of 1.0991 $Å^{-1}$ for CoF_2 and 1.0996 $Å^{-1}$ for ZnF_2. The data collection was monitored for instability by the measurement of six standard reflections every 94 reflections. The intensity fluctuations were less than 3% for both crystals.

[1] Supplementary data for this paper are available from the IUCr electronic archives (Reference: OS0063). Services for accessing these data are described at the back of the journal.

Table 1
Experimental details.

	CoF_2	ZnF_2
Crystal data		
Chemical formula	CoF_2	ZnF_2
Chemical formula weight	96.93	103.38
Cell setting, space group	Tetragonal, $P4_2/mnm$	Tetragonal, $P4_2/mnm$
a, b, c (Å)	4.6956 (5), 4.6956 (5), 3.1793 (3)	4.7038 (15), 4.7038 (15), 3.1336 (7)
α, β, γ (°)	90.000 (8), 90.000 (8), 90.000 (8)	90.00 (2), 90.00 (2), 90.00 (2)
V (Å^3)	70.099 (16)	69.33 (5)
Z	2	2
D_x (Mg m^{-3})	4.592	4.952
Radiation type	Synchrotron	Synchrotron
Wavelength (Å)	0.84	0.84
No. of reflections for cell parameters	6	6
θ range (°)	45.69–52.43	45.57–53.53
μ (mm^{-1})	18.22	26.55
Temperature (K)	293	293
Crystal form, colour	Rectangular, pink	Rectangular, clear
Crystal bounding faces	(100) × (010) × (001)	(110) × (1$\bar{1}$0) × (001)
Data collection		
Diffractometer	BL14A four circle	BL14A four circle
Data collection method	ω–2θ scans	ω–2θ scans
Peak scan width (ω, °)	0.5	0.6
Absorption correction	Analytical	Analytical
T_{min}	0.801	0.527
T_{max}	0.864	0.754
No. of measured and observed parameters	2883, 2502	2727, 2460
Criterion for observed reflections	$I > 2\sigma(I)$	$I > 2\sigma(I)$
No. of independent reflections	235	237
R_{int}, before and after absorption	0.0391, 0,0390	0.0404, 0.0402
θ_{max} (°)	67.41	67.47
Range of h, k, l	$-10 \rightarrow h \rightarrow 10$ $-10 \rightarrow k \rightarrow 10$ $-6 \rightarrow l \rightarrow 6$	$-10 \rightarrow h \rightarrow 10$ $-10 \rightarrow k \rightarrow 10$ $-6 \rightarrow l \rightarrow 6$
No. and frequency of standard reflections	6 every 94 reflections	6 every 94 reflections
Intensity decay (%), max	1.2	3.1
Refinement		
Refinement on	F	F
R, wR, S	0.019, 0.015, 2.416	0.014, 0.016, 2.388
No. of reflections and parameters used in refinement	235, 9	237, 9
Weighting scheme	$w = 1/\sigma^2(F)$	$w = 1/\sigma^2(F)$
$(\Delta/\sigma)_{max}$	0.00005	0.00013
$\Delta\rho_{max}$, $\Delta\rho_{min}$ (e Å^{-3})	1.166, −1.067	0.72, −0.679
$\sigma(\Delta\rho)$ (e Å^{-3})	0.11	0.08
Extinction method	Zachariasen (1967)	Zachariasen (1967)
Extinction coefficient	913 (85) ×10^1	327 (12) ×10^1
Extinction correction, y_{min} (hkl)	0.81, (110)	0.85, (110)

Computer programs used: *XtalDIFDATADDREFSORTRFABSORB, XtalCRYLSQ, XtalCIFIO* (Hall *et al.*, 1995).

The raw synchrotron data for CoF_2 and ZnF_2 was analysed for evidence of systematic errors such as obscuring the incident beam and Renninger effects. Several intensity measurements for both compounds deviating significantly from their equivalents were discarded in subsequent merging of equivalents procedure: 10 for the CoF_2 data set and 299 for the ZnF_2 data set, from periods of significant instability. Measured intensities were normalized using the incident beam intensities monitored during each scan. Integrated intensities were further modified and structure factor variances from counting statistics were adjusted for source instability, as indicated by the standards (Rees, 1977). Absorption corrections were evaluated analytically (Alcock, 1974). Further, symmetrically equivalent reflections were averaged and variances for reflections whose measures of variances prove unequal by a Fisher test were increased according to the scatter of equivalents. Table 1 lists R_{int} and parameters relevant to the absorption corrections.

3. Refinements

3.1. Spherical atom refinement

Six atomic displacement parameters, the fluorine positional parameter (x), Zachariasen's (1967) extinction parameter (r^*) and the structure factor scale (k) were determined for both compounds by full-matrix least-squares refinement based on $|F|$ weighted by $1/\sigma^2(F_o)$ for all measured structure factors of the CoF_2 and ZnF_2 data sets. The reference state was the independent atom model (IAM), evaluated using spherical atomic scattering factors from *International Tables for X-ray Crystallography* (1992, Vol. C). Dispersion corrections $\Delta f'$, $\Delta f''$ of 0.327 and 1.315 for Co, 0.125 and 1.914 for Zn, and 0.025 and 0.015 for F and atomic absorption coefficients (μ) in Table 1 at $\lambda = 0.84$ Å were evaluated by Creagh (1997). The *Xtal* (Version 3.4) suite of crystallographic programs (Hall *et al.*, 1995) was used running on DEC Alpha workstations. Details of the spherical atom data refinement are included in Table 1 and refined structural parameters are listed in Table 2.

3.2. Multipole refinement

A multipole refinement of the CoF_2 and ZnF_2 synchrotron diffraction data was performed using the program *VALRAY* (Stewart *et al.*, 1998). Input structure factors were already corrected for absorption and extinction after the IAM refinement. The total scale factor was not refined according to the approach pursued in *VALRAY*. It was estimated by the ratio of the sum of monopole populations over $F(000)$. Since

Table 2
Fractional coordinates and atomic displacement parameters U^{ij} (Å^2) and selected distances (Å) and angles (°) from IAM refinement.

		CoF_2	ZnF_2
Me (2*a*)	U^{11} (Å^2)	0.00685 (6)	0.00917 (4)
	U^{33} (Å^2)	0.00533 (7)	0.00763 (7)
	U^{12} (Å^2)	−0.00073 (5)	−0.00111 (3)
F (4*f*)	*x*	0.3034 (1)	0.3035 (1)
	U^{11} (Å^2)	0.01193 (16)	0.01307 (10)
	U^{33} (Å^2)	0.00803 (22)	0.01079 (17)
	U^{12} (Å^2)	−0.00529 (21)	−0.00515 (17)
Me −F		2.0149 (6)	2.0189 (6)
Me−F^{i}		2.0570 (4)	2.0405 (4)
F−Me−F^{i}		78.78 (2)	79.68 (2)

Symmetry code: (i) $x-\frac{1}{2}, \frac{1}{2}-y, \frac{1}{2}-z$.

the unit cell was kept electroneutral and the total amount of electrons was unchanged, the scale factor remained the same as in the IAM refinement. Multipoles allowed under the transition metal *mmm* and fluorine *m*2*m* site symmetries were selected according to the index-picking rules of Kurki-Suonio (1977). All allowed multipoles were included in the refinements, apart from the dipole parameter for fluorine, which was found to correlate too strongly with the fluorine positional parameter. It should be noted that Palmer & Jauch (1993) encountered the same problem with the F dipole term in their multipole refinements for NiF_2 and FeF_2.

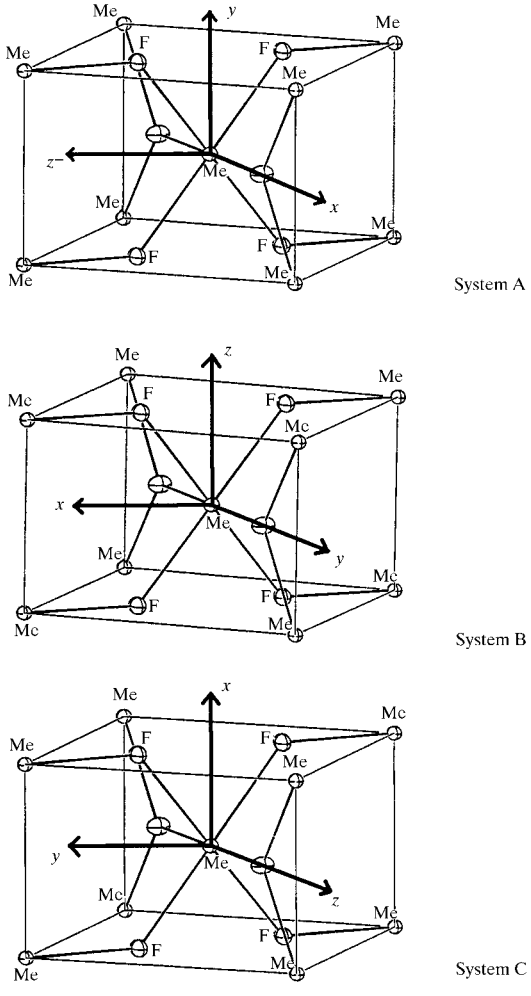

Figure 2
Coordinate system orientations for multipole refinements and 3*d*-orbital population calculations.

Table 3
Multipole refinement data.

	CoF_2		ZnF_2	
	Co	F	Zn	F
x		0.30341 (9)		0.30348 (7)
U^{11} (Å^2)	0.00678 (3)	0.01184 (17)	0.00894 (8)	0.01325 (9)
U^{33} (Å^2)	0.00521 (6)	0.00817 (27)	0.00784 (16)	0.01027 (15)
U^{12} (Å^2)	−0.00062 (6)	−0.00582 (28)	−0.00122 (7)	−0.00531 (16)
P_{00}	0.20 (8)	−0.10 (4)	−0.28 (6)	0.14 (3)
P_{20}	−0.065 (32)	0.073 (30)	0.087 (42)	−0.004 (25)
P_{22}	−0.005 (33)	0.024 (32)	−0.026 (60)	0.053 (35)
P_{30}		0.021 (26)		−0.012 (38)
P_{32}		−0.002 (25)		0.117 (41)
P_{40}	−0.091 (34)	−0.027 (32)	0.083 (39)	−0.032 (38)
P_{42}	0.267 (32)	0.021 (31)	0.125 (41)	0.069 (41)
P_{44}	0.174 (31)	−0.003 (32)	−0.049 (37)	−0.157 (49)
R (|*F*|)	0.0173		0.0128	
wR (|*F*|)	0.0124		0.0118	
S	2.006		1.792	
$F_{b,n-m}$	6.4		8.4	
$F_{b,n-m,\alpha}$ (α = 0.01)	2.2		2.2	

Three independent third-order anharmonic vibrational parameters (Johnson & Levy, 1974) for the F atom were included in early refinements, but were found to be insignificant in both data sets. Identical exponential radial density functions were utilized for each transition metal multipole. This less flexible approach was necessary for the subsequent calculation of 3*d*-orbital occupancies. The full ground-state atomic density was used as the 'core' density for each atom, so that the refined multipoles fitted the deformation density. This is similar to the approach introduced by Hirshfeld (1971). Multipole refinement parameters are listed in Table 3. A statistical *F* test ($F_{b,n-m} >> F_{b,n-m,\alpha}$) indicates that the increase of the number of parameters refined in this model compared with the IAM model in Table 1 significantly improve the fit to the experimental data, that is the decrease in *R* values and goodness-of-fit is statistically significant. The local coordinate system used for orientation of the transition metal multipoles is the system "C" illustrated in Fig. 2. No correlation coefficients greater than 0.7 were found between any two refined parameters. Structural parameters from the multipole refinements for the two compounds agree with those from the spherical atom refinement to within one or two standard uncertanties.

4. Results and discussion

4.1. Structural and atomic displacement parameters

The rutile-type structure is depicted in Fig. 1. Metal atoms are surrounded by a distorted octahedron of O or (as depicted) F atoms. In rutile (TiO_2) itself or other transition metal oxides there are two long contacts (labelled *B* in Fig. 1)

Table 4
Structural information for rutile-type fluorides.

Structural data used: MgF_2: Vidal *et al.* (1981), VF_2: Costa & de Almeida (1987), MnF_2: Naidu (1966), FeF_2: de Almeida *et al.* (1989), NiF_2: Palmer & Jauch (1993). The present data is used for CoF_2 and ZnF_2. Key: r_2: Me—F^i, r_4: Me—F^i, θ: F—Me—F^i.

	MgF_2	VF_2	MnF_2	FeF_2	CoF_2	NiF_2	ZnF_2
c/a	0.658 (1)	0.674 (7)	0.6793 (4)	0.7043 (1)	0.6771 (1)	0.6632 (4)	0.6662 (2)
r_2 (Å)	1.984 (1)	2.074 (3)	2.1043 (6)	2.002 (5)	2.0149 (6)	1.9806 (4)	2.0189 (6)
r_4 (Å)	1.994 (1)	2.092 (3)	2.1310 (5)	2.1177 (3)	2.0570 (4)	2.0215 (4)	2.0405 (4)
r_4/r_2	1.0050 (7)	1.009 (2)	1.0127 (4)	1.0577 (3)	1.0210 (4)	1.0206 (3)	1.0105 (4)
θ (°)	80.46 (8)	78.6 (2)	78.06 (2)	77.20 (2)	78.78 (2)	80.58 (2)	79.67 (2)

and four short (A) contacts, while in CoF_2 and ZnF_2 and other transition metal difluorides there are two short (B) and four long (A) contacts.

The cell dimensions for CoF_2 and ZnF_2 from Table 1 agree with previous room-temperature determinations by Stout & Reed (1954) and Naidu (1966) to within one standard uncertainty. Structural parameters reported in those early studies are of limited accuracy. Our results fall within their error bounds. There is good agreement between the present CoF_2 structural and atomic displacement parameters and those of the recent Costa *et al.* (1993) data sets.

The structural data in Table 2 show that the octahedron of F atoms coordinating cobalt in CoF_2 is more distorted than the corresponding F_6 octahedron in ZnF_2. There is a greater disparity between two short and four long Co—F contacts and the angles between contacts in the (110) plane deviate from 90° to a slightly greater extent in CoF_2. As mentioned before this greater distortion is attributed to the effects related to the repopulation of the unfilled Co 3*d* subshell in the crystal field.

In the light of some recent accurate diffraction studies, including the present one, it is instructive to conduct a phenomenological study of the structural distortions along the entire series of rutile-type transition metal fluorides, in the manner of Baur & Khan (1971). Table 4 lists some important structural data for this series of compounds. Structural distortions are greatest for compounds in the middle of the series, which contain transition metal atoms with almost half-filled 3*d*-subshells. Fig. 3, a bar plot of r_4/r_2 *versus* compound illustrates this point. The distortion is greatest for FeF_2 by a large margin. Interestingly r_4/r_2 and θ, both measures of the magnitude of the structural distortion, do not correlate well (Fig. 4). For example, NiF_2 has the θ angle close to the filled-subshell MgF_2 and ZnF_2 species, but a large r_4/r_2 ratio that is similar to the CoF_2 value. The difference between long and short contact distances and deviation from orthogonality in the (110) plane are thus separate effects. Updating a plot of Baur & Khan (Fig. 5), we see that there is little correlation between cell volume and c/a ratio for this series of compounds. As these authors point out, a purely spherical (ionic) form of bonding would result in a smooth curve, which is indeed found for rutile-type oxides containing metals with filled subshells. The deviations of CoF_2 and FeF_2 from the line connecting MgF_2 and ZnF_2 are particularly great. This was attributed by Baur & Khan to asymmetric distributions of *d* electrons. The physical evidence for such effects in terms of the electron density distribution is shown in the following section.

4.2. Electron density

Figs. 6 show the static deformation densities (Fourier summations of $F_{\rm multipole} - F_{\rm procrystal}$) from the multipole models in the (1$\bar{1}$0) and (002) planes for CoF_2 and ZnF_2. The CoF_2 residual density in the vicinity of atoms contains few features which are above the significance level in the experimental maps, indicating a good fit of the multipole model. Residual maps for ZnF_2 are relatively featureless apart from a roughly spherical accumulation of electron density left around the Zn atom. Attempts to reduce the magnitude of this feature during multipole refinement by adjustment of radial density functions and population parameters always resulted in the appearance of significant aspherical features in residual maps.

The static deformation density for CoF_2 shows pronounced asphericity in the electron density near Co atoms. Each Co atom is surrounded by six positive lobes with height up to 2.7 e Å^{-3} at a distance of ∼0.3 Å from the nucleus, which all

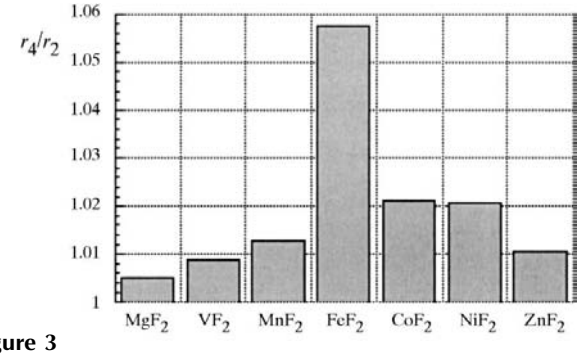

Figure 3
'Distortion indices' (r_4/r_2) for rutile-type transition metal fluorides.

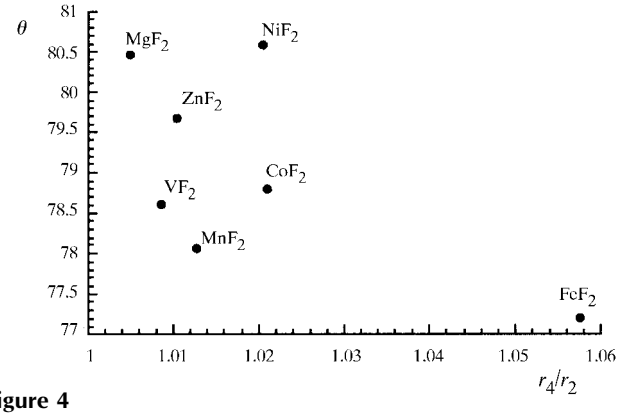

Figure 4
θ *versus* r_4/r_2 for rutile-type transition metal fluorides.

point in directions away from fluorine ligands. Depletions of density are found in the (002) section, directed to either side of the nearest F atoms. The density surrounding Co in the direction of the four long Co—F contacts is also negative, as seen in the (1$\bar{1}$0) section. The geometry and sign of density lobes are highly suggestive of preferential occupation of cobalt *d* orbitals. Explicit consideration of orbital occupation is made in the following section. The general behaviour of the observed density surrounding cobalt is consistent with the postulates of crystal field theory. All positive lobes of density are directed away from F ligands. In the (1$\bar{1}$0) section it is seen that positive lobes in the [001] direction are squeezed out into two positive lobes in the perpendicular (110) plane, because the [001] direction cuts through the narrower F—Co—F angle. Therefore, there are significant effects on the electron density resulting from the deviation of bond angles in the (110) plane from 90°.

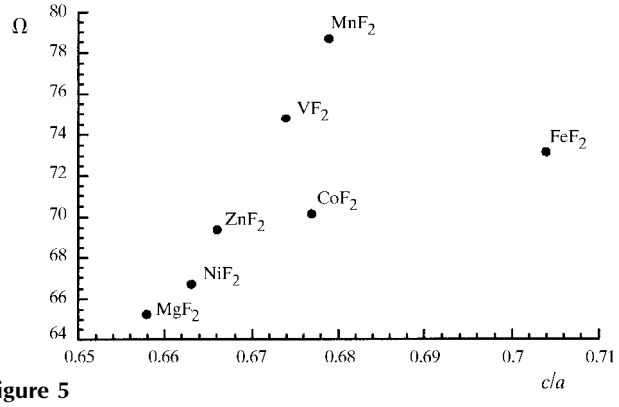

Figure 5
Cell volume Ω *versus* *c*/*a* for rutile-type transition metal fluorides.

Features around the F atom in Fig. 6(*a*) show a polarization of electron density in the direction of its nearest Co neighbour.

The electron densities for CoF_2 displayed by Costa *et al.* (1993) were obtained from separate experiments on two different CoF_2 crystals. These authors display dynamic deformation maps, so exact comparison with the present figures is inappropriate. However, it is worthwhile to note that the maps for one of the crystals show virtually no common features with the present maps. On the other hand, the other crystal's maps share many common qualitative features with the present static deformation densities. All the lobes of depleted density are oriented in the same manner and there are common positive lobes in the (1$\bar{1}$0) and (002) plane.

The static deformation density surrounding Zn in ZnF_2 possesses an approximate fourfold symmetry along the [001] direction, as seen in the (002) plane (Fig. 6*d*). This feature also appears to be in the (002) section of the theoretical electron density for ZnF_2 presented by Sorantin & Schwarz (1992). There is a notable accumulation of zinc electron density up to 2.8 e Å^{-3} at a distance of ∼0.15 Å from the nucleus directed

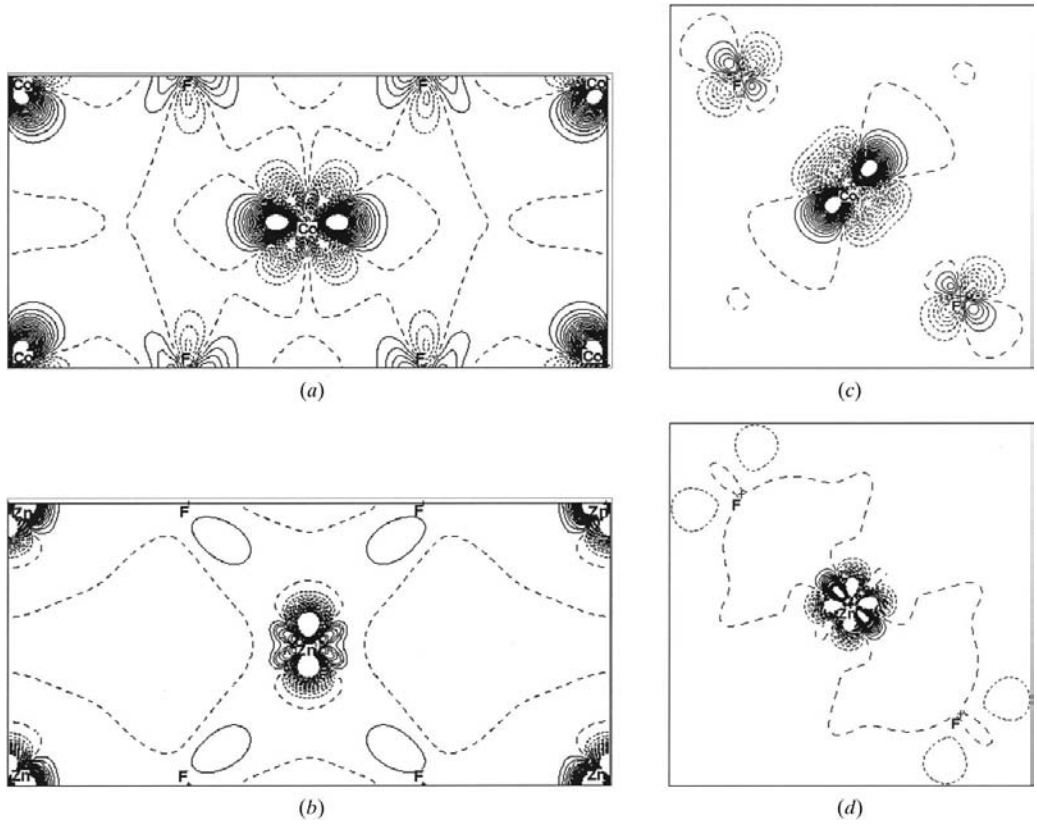

Figure 6
Multipole deformation density for (*a*) and (*c*) CoF_2, and (*b*) and (*d*) ZnF_2 in the (*a*) and (*b*) (1$\bar{1}$0) plane, and (*c*) and (*d*) (002) planes. Contour interval 0.1 e Å^{-3}, positive contours are solid and negative are shown as short dashed lines. Electron density is truncated at ±2 e Å^{-3}. Map borders: (*a*) and (*b*) 6.7 × 3.2 Å, and (*c*) and (*d*) 4.7 × 4.7 Å.

Table 5
3*d*-orbital populations from multipole refinement parameters.

		Spherical atom	System *A*	System *B*	System *C*
Co	d_{z^2}	1.4	1.9 (1)	1.4 (1)	1.2 (1)
	d_{xz}	1.4	1.2 (1)	1.2 (1)	1.8 (1)
	d_{yz}	1.4	1.2 (1)	1.8 (1)	1.2 (1)
	$d_{x^2-y^2}$	1.4	1.1 (1)	1.6 (1)	1.8 (1)
	d_{xy}	1.4	1.8 (1)	1.2 (1)	1.2 (1)
	$d_{z^2}d_{x^2-y^2}$	0.0	0.2 (1)	−0.7 (1)	0.5 (1)
Total Co 3*d* electrons: 7.20 (8)					
Zn	d_{z^2}	2.0	2.0 (2)	1.8 (2)	2.2 (1)
	d_{xz}	2.0	1.8 (2)	1.9 (1)	2.0 (2)
	d_{yz}	2.0	1.9 (2)	2.0 (1)	1.8 (2)
	$d_{x^2-y^2}$	2.0	1.9 (1)	2.2 (2)	1.8 (1)
	d_{xy}	2.0	2.0 (1)	1.8 (2)	1.9 (1)
	$d_{z^2}d_{x^2-y^2}$	0.0	−0.5 (2)	0.2 (2)	0.3 (2)
Total Zn 3*d* electrons: 9.72 (6)					

to the nearest F ligand. In the $(1\bar{1}0)$ section it is seen that as for CoF_2 density accumulates in the region of the wider F—Zn—F angle and is depleted from the smaller angle region. These observations are again consistent with crystal field theory, however, the accumulation of the zinc density towards its nearer F neighbour is an indication of a covalent-type interaction. Dynamic deformation density maps for ZnF_2 computed after spherical atom refinement (O'Toole, 1999) also show similar unusual features around the Zn atom, indicating the subtlety of bonding interactions for the filled $3d^{10}$ subshell of zinc.

General features of the static deformation density in these compounds can be related to the structural phenomena discussed in the previous section. The higher degree of asphericity surrounding Co, which was also noted in the dynamic deformation densities (O'Toole, 1999), is reflected in the greater distortion of the CoF_6 octahedron when compared to the ZnF_6 octahedron. As noted, the smaller θ angle for CoF_2 causes a split of positive density from between the narrowly spaced Co—F contacts in the $(1\bar{1}0)$ section and a sharp accumulation of density between the widely spaced contacts. This is responsible for the four main positive lobes of density in the CoF_2 (110) plane, seen at the corners of Fig. 6(*a*). Features around Zn cannot be so readily attributed to the deviation from orthogonality of the four Zn—F contacts in the $(1\bar{1}0)$ plane. Since the deviation from orthogonality (θ) correlates with the *c*/*a* ratio in rutile-type structures (Baur & Khan, 1971; O'Toole, 1999), we see the differing *c*/*a* ratio between CoF_2 and ZnF_2 reflected in their electron densities.

4.3. 3*d*-orbital populations

The refined multipole population parameters enable the calculation of relative *d*-orbital occupancies using the approach derived by Holladay *et al.* (1983). For the present metal point group *mmm* a 6 × 6 matrix is required to convert the six transition metal multipole parameters to populations of the five canonical *d* orbitals d_{z^2}, d_{xz}, d_{yz}, $d_{x^2-y^2}$ and d_{xy} plus a mixed term, $d_{z^2}d_{x^2-y^2}$. The mixed term has received no explicit discussion in previous calculations of this type for rutile-type structures. It is non-zero in this case because the *mmm* point group presents no symmetrically unique axis along which canonical *d* orbitals' *z* axes can be aligned. The $d_{z^2}d_{x^2-y^2}$ term, which integrates to zero, models those parts of the transition-metal atom density that deviate from 4*mm* symmetry. Calculated *d*-orbital occupancies will vary depending upon the coordinate system used for alignment of the refined multipoles. Table 5 is a summary of calculated *d*-orbital populations for each of the allowed local coordinate systems. Fig. 2 shows the orientation of each coordinate system, allowed according to the rules discussed by Kurki-Suonio (1977). The multipole parameters corresponding to system C are shown in Table 3. Multipole parameters that were computed using the other two coordinate systems are shown elsewhere (O'Toole, 1999). These refinements were identical to those discussed in the previous section, apart from the different coordinate system orientation.

Most of the shifts in 3*d*-orbital occupancies for Co in Table 5 are significantly different from zero, reflecting aspherical features observed in the deformation densities. The population shifts agree with expectations based on the known shape of *d*-orbitals and observed $\Delta\rho$ features when these are compared for each coordinate system orientation. The usefulness of the calculated 3*d* occupancies for Zn is limited, particularly because few changes in populations differ significantly from zero. However, note that the population for the mixed term in coordinate system *B* is not significantly different from zero. The *z* axis in coordinate system *B* is directed along the crystallographic *c* axis. It was observed earlier that this is the direction of an approximate fourfold rotation axis for the $\Delta\rho$ features around Zn. The 3*d*-orbital populations for Zn therefore confirm the approximate 4*mm* symmetry by the small mixed-term population for coordinate system *B* and larger mixed-term populations in other coordinate systems.

The extent of $d_{z^2} - d_{x^2-y^2}$ orbital mixing in *d* electron densities with point group *mmm* is smallest for those distributions with symmetry approaching 4*mm*, provided the *z* axis of the coordinate system used for multipole refinement is along the direction of the highest symmetry. It is intuitively desirable to favour a coordinate system orientation that yields small mixed *d*-orbital terms (system *A* for CoF_2 and system *B* for ZnF_2), because the natural basis orbitals in these cases closely resemble the familiar canonical *d* orbitals. When these systems are adopted, the results of orbital population calculations can be readily compared with those of lower point symmetry systems for which the canonical *d* orbitals *are* the conventional, unambiguous basis for the *d*-orbital density. Of course, no extra information on the distribution of atomic electrons is extracted from such an approach.

The only published 3*d*-orbital populations calculated from multipole refinement parameters for the present structures are in the CoF_2 study of Costa *et al.* (1993). It is difficult to reconcile their results with the values found in the present study because these authors do not indicate the coordinate system used and the mixed $d_{z^2}d_{x^2-y^2}$-orbital populations. There is little agreement between the Costa *et al.* populations and the values in Table 5 for any coordinate system.

Table 6
3*d*-orbital populations from multipole refinement of Palmer & Jauch (1993) and from theoretical calculation of Valerio *et al.* (1995) for FeF_2.

	Palmer & Jauch (1993)	Valerio *et al.* (1995)
d_{z^2}	1.15 (12)	1.092
d_{xz}	0.88 (11)	1.011
d_{yz}	0.95 (11)	1.011
$d_{x^2-y^2}$	1.90 (13)	1.966
d_{xy}	1.04 (13)	1.045

The close qualitative agreement between the experimental electron density of Palmer & Jauch (1993) and the theoretical density of Valerio *et al.* (1995) for FeF_2 should be reflected in the 3*d*-orbital populations reported in these studies. Palmer and Jauch's multipole refinement of γ-ray diffraction data was performed using coordinate system C. Valerio *et al.* (1995) list Mulliken population data for iron 3*d*-orbitals with a coordinate system in which the *x* and *y* axes of system C are rotated by 45°. It is relatively straightforward to show that such a transformation exchanges the d_{xy} and $d_{x^2-y^2}$ populations and leaves the others unchanged, provided the populations of d_{xz} and d_{yz} are equal. Performing the necessary conversions enables direct comparison of the data from the two studies (Table 6). This is an impressive agreement between experiment and theory, indicating the potential of experimental *d*-orbital population refinements for comparison with theories of electronic structure. Unfortunately, there is no explicit consideration of the mixed $d_{z^2}d_{x^2-y^2}$-orbital in either of these studies. Had the d_{xz}- and d_{yz}-orbital occupancies of Valerio *et al.* (1995) not been equal, the conversion of their values to the above setting would have required knowledge of the mixed term population. To facilitate easy comparison of data from different sources it is desirable that unambiguous definition of coordinate systems and explicit consideration of all orbital populations be made in calculations of this type for point groups of symmetry *mmm* and lower.

5. Conclusions

Static deformation densities obtained after multipole refinement against the experimental synchrotron X-radiation data clearly show the redistribution of metal electrons based on the geometry of the ligand field. There is also an indication of Co—F interactions, with a polarization of fluorine density towards its nearest neighbour. There are little significant features near F in the ZnF_2 deformation density, which is dominated by the distribution surrounding Zn. The nature of bonding in ZnF_2 and other $3d^{10}$ compounds, which includes orbital hybridization between metal and ligands (Dunitz & Orgel, 1960), means that the simple atom-centred density functions used in multipole models may not be adequate to fully describe electronic interactions in these materials. Several other bonding effects in these structures, such as metal–metal and ligand–ligand bonding, have been related to the lattice geometry after theoretical band structure calculations (*e.g.* Sorantin & Schwarz, 1992). It is difficult to attribute any qualitative features of the present densities to such interactions. The electron densities derived from theoretical calculations can be meaningfully compared with the present experimental $\Delta\rho$ distributions. However, it appears that much information on bonding orbitals obtained in theoretical studies, while implicit in theoretical electron densities, cannot be easily extracted from experimental distributions. Our confidence in such bonding information is increased when there is accord between theoretically and experimentally derived electron-density distributions.

The authors would like to acknowledge the valuable support of the late Dr E. N. Maslen during the early stages of this research. This work was supported by the Australian Research Council. Financial support from the Australian Synchrotron Research Program funded by the Commonwealth of Australia *via* the Major National Research Facilities Program is also acknowledged.

References

Alcock, N. W. (1974). *Acta Cryst.* A**30**, 332–335.
Almeida, M. J. M. de, Costa, M. M. R. & Paixao, J. A. (1989). *Acta Cryst.* B**45**, 549–555.
Baur, W. H. & Khan, A. A. (1971). *Acta Cryst.* B**27**, 2133–2139.
Burdett, J. K. (1995). *Acta Cryst.* B**51**, 547–558.
Burdett, J. K. & Eisenstein, O. (1992). *Inorg. Chem.* **31**, 1758–1766.
Costa, M. M. R. & de Almeida, M. J. M. (1987). *Acta Cryst.* B**43**, 346–352.
Costa, M. M. R., Paixao, J. A., de Almeida, M. J. M. & Andrade, L. C. R. (1993). *Acta Cryst.* B**49**, 591–599.
Creagh, D. C. (1997). Personal communication.
Dovesi, R., Saunders, V. R. & Roetti, C. (1992). *CRYSTAL*92 *User's Manual*. Gruppo di Chim Teorica, Université di Torino, Italy.
Dunitz, J. D. & Orgel, L. E. (1960). *Adv. Inorg. Chem. Radiochem.* **2**, 1–48.
Hall, S. R., King, G. S. D. & Stewart, J. M. (1995). *Xtal*3.4 *User's Manual*. University of Western Australia, Australia.
Hirshfeld, F. L. (1971). *Acta Cryst.* B**27**, 769–781.
Holladay, A., Leung, P. & Coppens, P. (1983). *Acta Cryst.* A**39**, 377–387.
Johnson, C. K. & Levy, H. A. (1974). *International Tables for X-ray Crystallography*, Vol. IV, pp. 314–319. Birmingham: Kynoch Press.
Kishimoto, S., Ishizawa, N. & Vaalsta, T. P. (1998). *Rev. Sci. Instrum.* **69**, 384–391.
Kurki-Suonio, K. (1977). *Isr. J. Chem.* **16**, 115–123.
Naidu, S. V. N. (1966). Ph.D. thesis. Osmania University, India.
Niederauer, K. & Göttlicher, S. (1970). *Z. Angew. Phys.* pp. 16–21.
O'Toole, N. (1999). Ph.D. thesis. The University of Western Australia, Australia.
Palmer, A. & Jauch, W. (1993). *Phys. Rev. B*, **49**, 10304–10310.
Rees, B. (1977). *Isr. J. Chem.* **16,** 180–186.
Satow, Y. & Iitake, Y. (1989). *Rev. Sci. Instrum.* **60**, 2390–2393.
Shintani, H., Sato, S. & Saito, Y. (1975). *Acta Cryst.* B**31**, 1981–1982.
Sorantin, P. I. & Schwarz, K. (1992). *Inorg. Chem.* **31**, 567–576.
Stewart, R. F., Spackman, M. A. & Flensburg, C. (1998). *Valray*98 *Reference Manual*. University of Copenhagen, Denmark.
Stout, J. W. & Reed, A. (1954). *J. Am. Chem. Soc.* **76**, 5279.
Streltsov, V. A. & Ishizawa, N. (1999). *Acta Cryst.* B**55**, 321–326.
Streltsov, V. A., Ishizawa, N. & Kishimoto, S. (1998). *J Synchrotron Rad.* **5**, 1309–1316.
Valerio, G., Catti, M., Dovesi, R. & Orlando, R. (1995). *Phys. Rev. B*, **52**, 2422–2427.
Vidal, J. P., Vidal-Valat, G., Galtier, M. & Kurki-Suonio, K. (1981). *Acta Cryst.* A**37**, 826–837.
Zachariasen, W. H. (1967). *Acta Cryst.* **23**, 558–564.